J Mol Model (2011) 17:3027–3038
DOI 10.1007/s00894-011-0995-6

ORIGINAL PAPER

Effects of nanoparticles on the compatibility of PEO-PMMA block copolymers

Dan Mu · Jian-Quan Li · Wei-Dong Li · Song Wang

Received: 12 December 2010 / Accepted: 26 January 2011 / Published online: 1 March 2011

Abstract The compatibility of six kinds of designed poly (ethylene oxide)-block-poly(methyl methacrylate) (PEO-b-PMMA) copolymers was studied at 270, 298 and 400 K via mesoscopic modeling. The values of the order parameters depended on both the structures of the block copolymers and the simulation temperature, while the values of the order parameters of the long chains were higher than those of the short ones; temperature had a more obvious effect on long chains than on the short ones. Plain copolymers doped with poly(ethylene oxide) (PEO) or poly(methyl methacrylate) (PMMA) homopolymer showed different order parameter values. When a triblock copolymer had the same component at both ends and was doped with one of its component polymers as a homopolymer (such as A5B6A5 doped with B6 or A5 homopolymer), the value of its order parameter depended on the simulation temperature. The highest order parameter values were observed for A5B6A5 doped with B6 at 400 K and for A5B6A5 doped with A5 at 270 K. A study of copolymers doped with nanoparticles showed that the mesoscopic phase was influenced by not only the properties of the nanoparticles, such as the size and density, but also the compositions of the copolymers. Increasing the size of the nanoparticles used as a dopant had the most significant effect on the phase morphologies of the copolymers.

Keywords PEO-b-PMMA copolymer · Computer simulation · Nanoparticle effect

D. Mu (✉) · W.-D. Li
Department of Chemistry and Chemical Engineering,
Zaozhuang University,
Shandong 277160, China
e-mail: mudanjlu1980@yahoo.com.cn

J.-Q. Li
Physics & Electronic Engineering Department,
Zaozhuang University,
Shandong 277160, China

S. Wang
Institute of Theoretical Chemistry, State Key Laboratory
of Theoretical and Computational Chemistry, Jilin University,
Changchun, 130023, China

Introduction

Because of their inherent beauty and potential technological applications, the molecular self-assembly of block copolymers to form nanostructured materials is an active area of research. Thin films of self-organizing diblock copolymers may be suitable for semiconductor applications since they enable the ordered domains to present ordered patterns with dimensions that are below photolithographic resolution in wafer-scale areas [1]. Block copolymers are known to generate nanoscale microdomains by microphase separation if they are annealed at temperatures lower than their order–disorder transition temperatures [2]. Recently, thin films formed by block copolymers with well-defined nanostructures have received considerable attention due to their potential nanofabrication applications [3–10]. In these applications, the ability to control the morphology of the block copolymer thin film by adjusting various influential factors in order to obtain an ordered phase-separated microdomain has potential significance.

PEO and PMMA are both important polymers for synthesis and for applications in a variety of engineering and biomedical areas [11–13]. The study of PEO/PMMA blends is of interest because of the semicrystalline nature of PEO, the weak interactions between these two polymers, and the large difference in their glass transition temperatures (*Tg*), which mean that such blends are complex systems. Our previous paper successfully clarified the conflicting conclusions drawn from different laboratories and from different techniques from a theoretical viewpoint. We found that the blends tended to undergo microphase

separation at higher temperatures such as 400 K, while PEO/PMMA blends were miscible at lower temperatures [14].

Amphiphilic graft and block copolymers made of PMMA and PEO blocks have received increasing attention due to their potential applications in keratoprosthesis modification [15], drug carriers [16], and biomedical materials [17, 18]. The copolymer PEO-b-PMMA is of interest because of its crystallization behavior, and Sun et al. reported that the crystallization rate and the degree of crystallinity decreased with increasing PMMA content [19], which means that the PEO block in the PEO-b-PMMA copolymer tends to crystallize. Furthermore, there are no reports on the effects of nanoparticles on the PEO-b-PMMA copolymer. We gained some useful results in the work reported in the current paper that can be applied to nanofabrication to improve its function.

Simulation details

Mesoscale structures are of the utmost importance during the production processes of many materials, such as polymer blends, block copolymer systems, surfactant aggregates in detergent materials, latex particles and drug delivery systems. Mesoscopic dynamics models are receiving increasing attention, as they form a bridge between microscale and macroscale properties [20–23]. Our simulation processes were all carried out with the MesoDyn package in the Materials Studio commercial software provided by Accelrys on an SGI workstation. MesoDyn is a state-of-the-art mesoscale simulation program. It utilizes a dynamic variant of mean-field density functional theory with Langevin-type equations to investigate polymer diffusion, providing a coarse-grained method for the study of complex fluids, their kinetics, and their equilibrium structures at large length and time scales. The thermodynamic forces are found via mean-field DFT, using the Gaussian chain as a model (see also the discussion of the dynamics and themodynamics of MesoDyn provided in the "Appendix"). The coarse-grained Gaussian chain consists of beads with equal lengths and equal volumes. When the free energy of the system remains stable with increasing simulation time, the phase separation is complete.

The order parameter, P, is defined as the average volume of the difference between the local density squared and the overall density squared, as given by the equation

$$P_i = \frac{1}{V}\int_V \left[\eta_i^2(r) - \eta_i^2\right] dr,$$

where η_i is the dimensionless density (volume fraction) of species i. The larger the value of P, the greater the phase separation. A decrease in P indicates better compatibility or miscibility, and the polymer phases mix more randomly.

The modeling reported in this paper can be divided into two main parts. In the first part, six PEO-b-PMMA copolymers with different chain lengths and arrangements were designed in order to study their compatibility at various temperatures. In the second part, seven different PEO-b-PMMA copolymers doped with nanoparticles in various configurations were designed in order to study the effects of the properties of the nanoparticles on the phase morphologies of the PEO-b-PMMA copolymers.

Modeling undoped PEO-b-PMMA copolymers

In order to study the compatibility of different PEO-b-PMMA copolymers, six PEO-b-PMMA copolymers—denoted A5B6, A10B12, A5B6A5, A10B12A10, B6A5B6 and B12A10B12—were designed (here, A and B represent PEO and PMMA blocks, respectively). For convenience, A5B6 and A10B12 were collectively defined as the "AB" group; A5B6A5 and A10B12A10 were defined as the "ABA" group; and B6A5B6 and B12A10B12 were defined as the "BAB" group. The first member of each group has short PEO-b-PMMA chains and the second member has long ones (twice as long as those in the first member).

Modeling PEO-b-PMMA copolymers doped with either PEO or PMMA

These models were divided into two types according to the component (either PEO or PMMA homopolymer) was doped into the PEO-b-PMMA copolymer. The chain length of the dopant homopolymer was the same as that of its counterpart in the PEO-b-PMMA copolymer.

The first type consisted of six models doped with component A: A5B6 doped with A5, A10B12 doped with A10, A5B6A5 doped with A5, A10B12A10 doped with A10, B6A5B6 doped with A5, and B12A10B12 doped with A10. The second type comprised six copolymers doped with component B: A5B6 doped with B6, A10B12 doped with B12, A5B6A5 doped with B6, A10B12A10 doped with B12, B6A5B6 doped with B6, and B12A10B12 doped with B12.

Modeling PEO-b-PMMA copolymers doped with nanoparticles

Seven different systems (or "cases") of PEO-b-PMMA copolymer doped with column-shaped nanoparticles were built. Table 1 lists these systems along with the number of nanoparticles in each layer (N_p), the radius of each nanoparticle (r_p), the height of each nanoparticle (h_p), the number of layers (N_L) and the total number of nanoparticles added as dopant (N_{tp}). Among these cases, case 1 (the 4-3-4-2 system, with four nanoparticles in each layer, a

Table 1 The seven nanoparticle-doped PEO-b-PMMA copolymer systems that were modeled in this work

Case	System	N_p	r_p (nm)	h_p (nm)	N_L	N_{tp}
1	4-3-4-2	4	3	4	2	8
2	4-3-4-3	4	3	4	3	9
3	4-3-4-4	4	3	4	4	16
4	4-3-8-2	4	3	8	2	8
5	4-3-8-3	4	3	8	3	9
6	4-6-8-2	4	6	8	2	8
7	8-3-4-2	8	3	4	2	16

nanoparticle radius of 3 nm, a nanoparticle height of 4 nm, and two layers) was used as the base case; in other words, all of the other cases were derived from it. Adding one more nanoparticle to the center of the base case yielded case 2 (the 4-3-4-3 system); increasing the number of layers to four without changing any other settings produced case 3 (the 4-3-4-4 system); doubling the nanoparticle height led to case 4 (the 4-3-8-2 system); adding one more nanoparticle to the middle of the simulation box in case 4 to increase the number of layers to three gained case 5 (the 4-3-8-3 system); doubling the nanoparticle radius in case 4 produced case 6 (the 4-6-8-2 system); and doubling the nanoparticle density of every layer in case 1 yielded case 7 (the 8-3-4-2 system). Figure 1 shows the schemes for these seven cases. The input parameters were the same as those used in the previous mesoscopic simulations performed at 270, 298 and 400 K, and a total simulation time of 10 ms was applied in each case. The six PEO-b-PMMA copolymers described above (A5B6, A10B12, A5B6A5, A10B12A10, B6A5B6, and B12A10B12) were modeled in each case. Thus, the main objective of modeling these cases was to determine the factor that exerted the most influence on phase separation: the size, the number, the density, or the arrangement of the nanoparticles. However, we also explored the effect of varying the temperature on the phase separation.

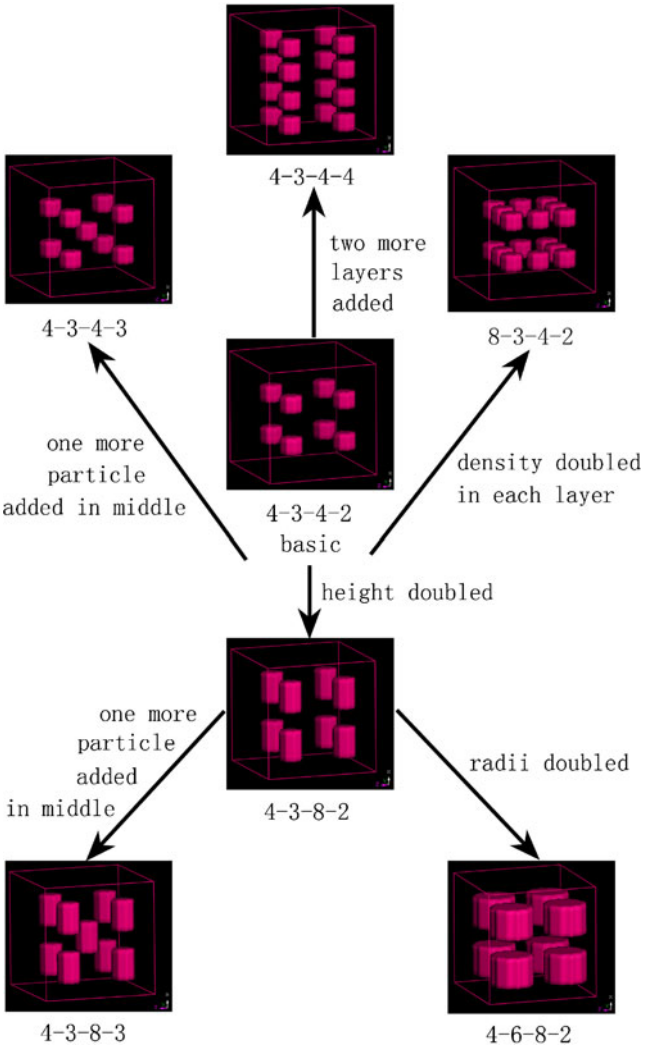

Fig. 1 The seven nanoparticle configurations studied in this work

Modeling PEO-b-PMMA copolymers doped with nanoparticles, PEO, and PMMA

Expanding upon the previous modeling, we then considered the seven nanoparticle-doped copolymer systems described above but with two extra dopants: PEO and PMMA. As we did in the investigation of PEO-b-PMMA copolymers doped with either PEO or PMMA, we tested weight percentages of 18%, 33%, 55% and 67% PEO-b-PMMA. We also varied the simulation temperature (modeling was performed at 270 and 400 K) in order to permit comparison with the modeling results obtained for the seven nanoparticle-doped copolymer systems without PEO and PMMA dopants. The PEO and PMMA dopants that were added had the same chain lengths as their corresponding homopolymers; thus, we modeled A5B6 doped with A5 and B6, A10B12 doped with A10 and B12, A5B6A5 doped with A5 and B6, A10B12A10 doped with A10 and B12, B6A5B6 doped with A5 and B6, and B12A10B12 doped with A10 and B12.

Results and discussion

Modeling results for undoped PEO-b-PMMA copolymers

Figure 2 shows the modeling results for undoped ("plain") PEO-b-PMMA copolymers. There are several features of this figure that are worth noting:

(1) The P values of the copolymers with long chains (A10B12, B12A10B12 and A10B12A10) were all

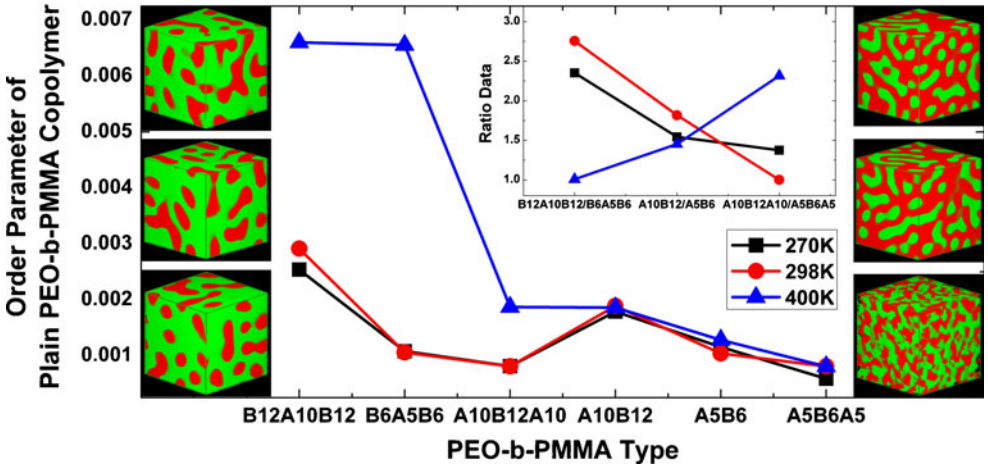

Fig. 2 *P* values of six types of PEO-b-PMMA copolymer at different temperatures. The *three pictures on the left* are the phase morphologies of the B12A10B12 triblock copolymer at 270 (*top*), 298 (*middle*) and 400 K (*bottom*). The *three pictures on the right* are the phase morphologies of the A5B6A5 triblock copolymer at 270 (*top*), 298 (*middle*) and 400 K (*bottom*), where "A" and "B" represent PEO and PMMA blocks, respectively

higher than those of the copolymers with short ones (A5B6, B6A5B6 and A5B6A5), respectively, which meant that the long PEO-b-PMMA copolymers were more likely to undergo microscopic phase separation. The order of *P* values at 400 K was A10B12>A5B6, B12A10B12>B6A5B6 and A10B12A10>A5B6A5, which suggests that when the "A" and "B" blocks of the long-chain polymers are both long enough, microscopic areas consisting of just one component appear, and microscopic separation could even occur.

(2) The order of *P* values at 270 and 298 K was the same, but it changed at 400 K. This could be due to different compatibilities of the PEO/PMMA blends at different temperatures. In our previous work, we found that the PEO/PMMA blends tend to undergo microphase separation at high temperatures such as 400 K, while the blends were miscible at lower temperatures such as 270 and 298 K [14]. Therefore, the *P* values of the PEO-b-PMMA copolymers at 270 and 298 K were lower than the *P* value at 400 K for the same copolymer type, especially for the B12A10B12, B6A5B6 and A10B12A10 triblock copolymers.

(3) The inset in Fig. 2 shows the ratio (denoted *R*) of the *P* values of the two members of each copolymer group at three temperatures. In this case, *R* always corresponds to the *P* value of the long-chain member divided by the *P* value of the short-chain member. For example, for the "AB" group, the *R* value is the *P* value of A10B12 divided by the *P* value of A5B6. The order of *R* values at 400 K was very different from those at 270 and 298 K: "ABA" group>"AB" group >"BAB" group at 400 K, whereas "BAB" group>"AB" group>"ABA" group at 270 and 298 K. Based on the *R* values, it is clear that, at 400 K, increasing the chain length greatly affected the *P* value in the "ABA" group, while it had little effect in the "AB" and "BAB" groups. On the contrary, at 270 and 298 K, increasing the chain length greatly affected the *P* value of the "BAB" group, while it did not have a large effect in the "AB" and "ABA" groups. This is mainly because the "ABA" and "BAB" groups have "A" or "B," respectively, at both ends of the copolymer, meaning that when neighboring copolymer molecules make contact, that contact is much more likely to occur between the same components (e.g., "A" on one molecule with "A" on the other) than is the case for "AB" group molecules. In addition, the PEO block tends to crystallize at low temperatures, and PMMA starts to soften at the glass transition temperature (*Tg*=378 K),but does not extensively depolymerize until 453 K [24]. Therefore, increasing the chain length had different effects on the *P* and *R* values depending on the simulation temperature. Based on the differences between *P* values at different temperatures, it is clear that the "BAB" group is more sensitive to changes in temperature than the other two groups.

Modeling results for PEO-b-PMMA copolymers doped with either PEO or PMMA

Subfigures a1, a2, a3 and a4 in Fig. 3 show the *P* values for the six different PEO-b-PMMA copolymers doped with either PEO or PMMA at two temperatures (270 and 400 K). Subfigures b1, b2, b3 and b4 show the corresponding *R* values for these doped copolymers, where the *R* values on this occasion are defined as the *P* value of the copolymer with dopant divided by the *P* value of the undoped copolymer. A reference line is drawn through $R = 1$ in subfigures b1, b2, b3 and b4. When an *R* value lies above this line, the doping can be considered to have a reinforcing effect; otherwise, the doping can be considered to have a weakening effect. The plots show the weight percentage of

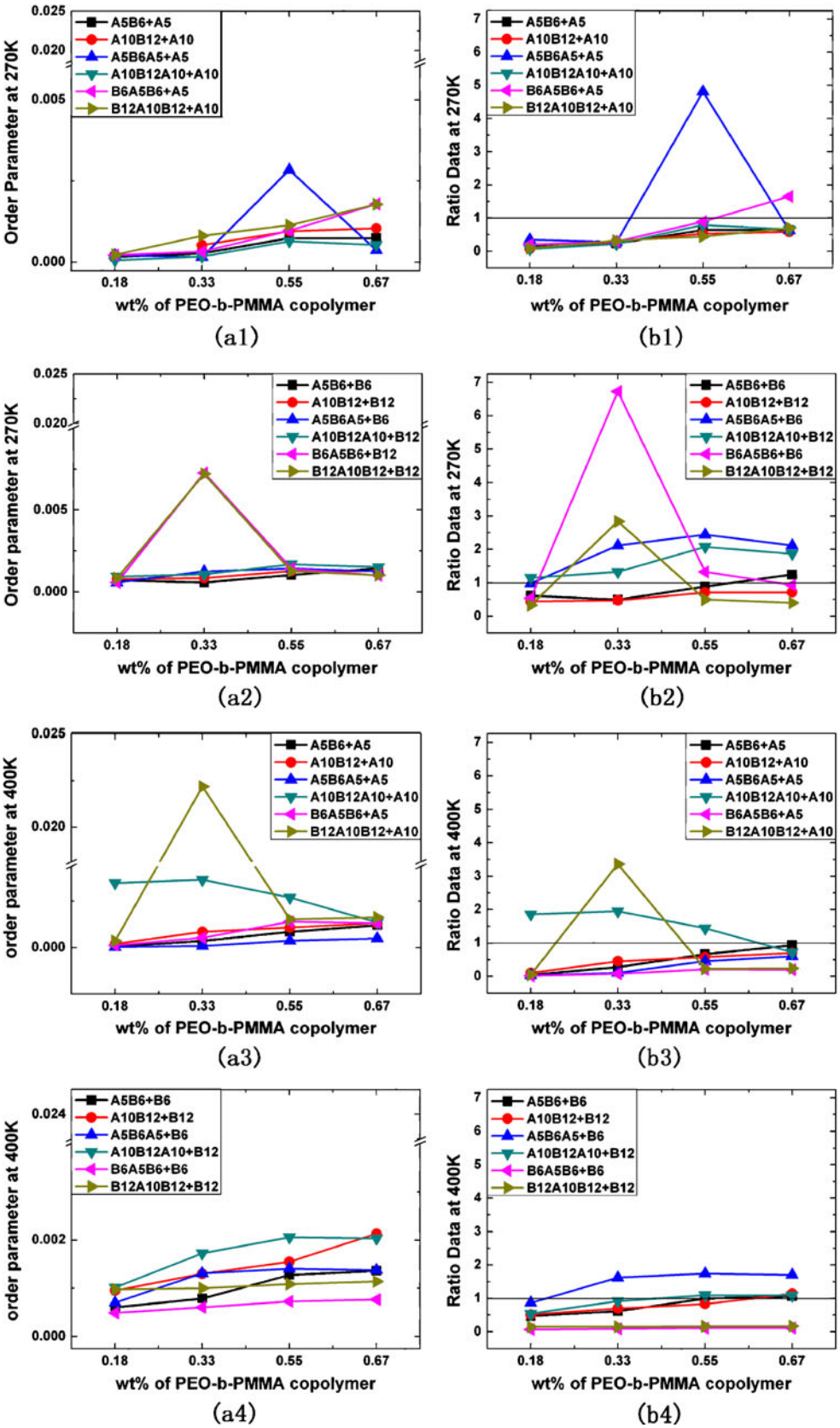

Fig. 3 *P* and *R* values of PEO-b-PMMA copolymers doped with either PEO or PMMA at 270 or 400 K, respectively

the PEO-b-PMMA copolymer along the *x* axis; weight percentages of 18%, 33%, 55% and 67% were chosen as examples. The following features of the plots are noteworthy:

(1) Subfigure a1 is similar to subfigure b1, and subfigure a2 is similar to subfigure b2, which means that the strength of the effect of doping with either PEO or PMMA at 270 K is almost directly proportional to the amount of dopant. This is also the case at 400 K.

(2) Subfigures b1 and b2 show the *R* values at 270 K. The *R* values for 18, 33, 55 and 67% PEO-b-PMMA copolymer doped with PEO in subfigure b1 were all below the reference line, except in the cases of A5B6A5 doped with A5 and B6A5B6 doped with A5. This means that the doping had a weakening effect in most cases. When there was a relatively large amount of PEO, as in the systems doped with 18% and 33% PEO-b-PMMA copolymer, the whole system tended to be more miscible, like pure PEO (noting that PEO tends to crystallize at low temperature). As the copolymer fraction increases, the amount of PEO decreases, so only two cases show a reinforcing effect: 55% A5B6A5 doped with A5 and 67% B6A5B6 doped with A5. However, subfigure b2 shows markedly different results from b1: there are many more systems in subfigure b2 that show a reinforcing effect of doping compared with those in subfigure b1; in particular, the *R* value for 33% B6A5B6 doped with B6 is extremely high. The *R* values for the "AB" group are below the reference line, indicating a weakening effect of doping, except in the case of 67% A5B6 doped with B6. The *R* values of the "ABA" group are all above the reference line, suggesting a reinforcing effect of doping; also, as the amount of PEO-b-PMMA copolymer increases, the *R* value increases, especially when the amount changes from 18% to 33%, although there was no obvious change in *R* when there was a relatively large amount of copolymer, as in the systems with 55% and 67% copolymer. Only three *R* values for the "BAB" group were above the reference line: those for 33% B6A5B6 doped with B6, 33% B12A10B12 doped with B12, and 55% B6A5B6 doped with B6, which showed reinforcing effects of the doping. Thus, the other cases in the "BAB" group showed weakening effects of the doping. The reason for the two outstandingly high *R* values for 33% B6A5B6 doped with B6 and 33% B12A10B12 doped with B12 is that the "B" component of the copolymer in these systems links to the doped B6 or B12 homopolymer to form an area of "B" components when the proportion of copolymer is 33%. In addition, the length of B6A5B6 is half that of B12A10B12, which means that B6A5B6 is more maneuverable than B12A10B12 and thus more adept at changing position, resulting in an ordered domain or even an ordered phase morphology. Thus, the *R* values for B6A5B6 doped with B6 were much higher than those for B12A10B12 doped with B12.

(3) Subfigures b3 and b4 show the *R* values at 400 K, which are very different to those observed at 270 K. The *R* values of 18%, 33%, 55% and 67% PEO-b-PMMA copolymer doped with PEO in subfigure b3 were all below the reference line, except for 18%, 33% and 55% A10B12A10 doped with A10 and 33% B12A10B12 doped with A10, which meant that most cases showed a weakening effect of doping. The systems with 33%, 55% and 67% A5B6A5 doped with B6 all presented outstandingly high *R* values, while the *R* values of other systems were below or close to the reference line. In summary, at 400 K, when a particular proportion of a triblock copolymer with the same component at both ends was doped with a homopolymer consisting of the same component as that present in the middle of the triblock copolymer—such as B12A10B12 doped with A10 or A5B6A5 doped with B6—it gave a high *R* value. Taking the system comprising A5B6A5 copolymer doped with B6 as an example, the reason for this result was that its "A" component would prevent the B6 homopolymer dopant from approaching the "B" group in the middle of the A5B6A5 copolymer due to the heterogeneity between the "A" and "B" components. In addition, the temperature of 400 K was high enough to prevent the semicrystallization of the PEO component.

Modeling results for PEO-b-PMMA copolymers doped with nanoparticles

Figure 4 shows the *P* values of PEO-b-PMMA copolymers doped with nanoparticles in various configurations. The *y* axes (corresponding to order parameter values) of the six subfigures in Fig. 4 all range from 0.0007 to 0.011, which allows the data in the different subfigures to be compared more easily. In each subfigure, the *P* values at 400 K are arranged in ascending order. Some notable features of the subfigures in Fig. 4 are discussed below:

(1) The trend in *P* values as the temperature was increased from 270 to 298 to 400 K was the same for all of the PEO-b-PMMA copolymers. Furthermore, the order of *P* values for the different nanoparticle systems was the same at 270, 298, and 400 K: 4682>8342>4344>4383>4382>4343>4342, which indicates that a more ordered phase morphology can be obtained by increasing the density, size and number of nanoparticles used for doping.

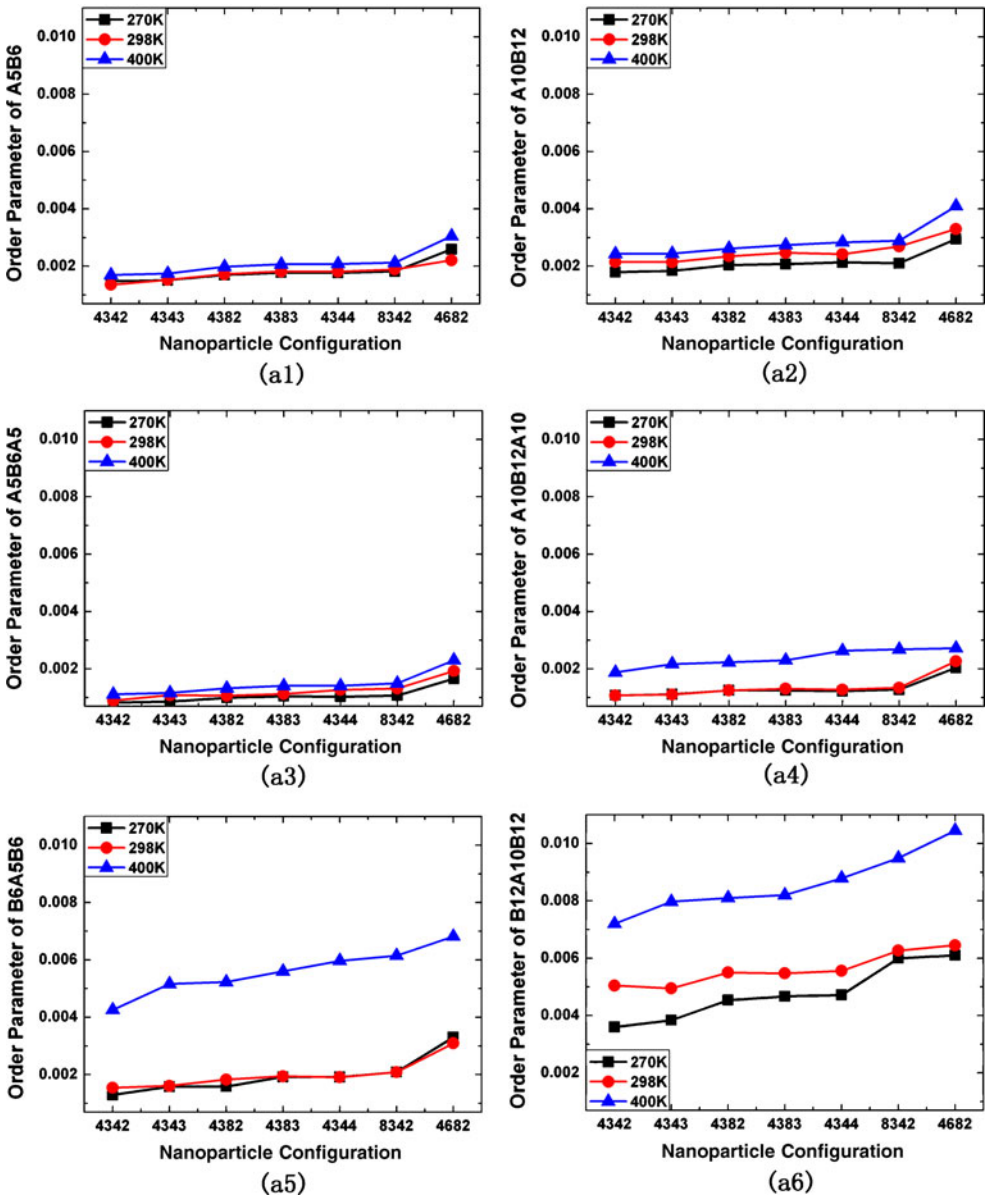

Fig. 4 *P* values of six kinds of PEO-b-PMMA copolymer doped with nanoparticles in various configurations at 270, 298 and 400 K, respectively

(2) The variations in the *P* values of the PEO-b-PMMA copolymers at different temperatures show that the temperature has a strong effect on triblock copolymers with long chains (A10B12A10, B6A5B6 and B12A10B12), but hardly any effect on short diblock and triblock copolymer chains (A5B6, A10B12 and A5B6A5). This may be linked to the chain length, because the longer the chain, the harder it is for it to move. Furthermore, the *P* values at 400 K were higher than the corresponding ones at 270 and 298 K. Also, the difference in the *P* values for 270 and 298 K for the same kind of copolymer was very small, which meant that increasing the temperature had an obvious effect on the phase morphology, especially for longer copolymers.

Figure 5 shows the corresponding *R* values of the copolymers doped with nanoparticles. Here, the *R* value is defined as the *P* value of the PEO-b-PMMA copolymer doped with nanoparticles divided by the *P* value of the corresponding undoped PEO-b-PMMA copolymer. The *y* axes of the six subfigures in Fig. 5 all ranged from 0.5 to 3.25 to make it easier to compare the data from different subfigures. In each subfigure, the *R* values of these six kinds of PEO-b-PMMA copolymer at 400 K are arranged in ascending order to permit easy comparison with Fig. 4. Indeed, Figs. 4 and 5 are similar in terms of the shapes of the curves in the six subfigures, as well as in the order of *R* values: 4682>8342>4344>4383>4382>4343>4342. However, the order of *R* values at 270 K and the order at 298 K were not exactly the same as seen at 400 K in

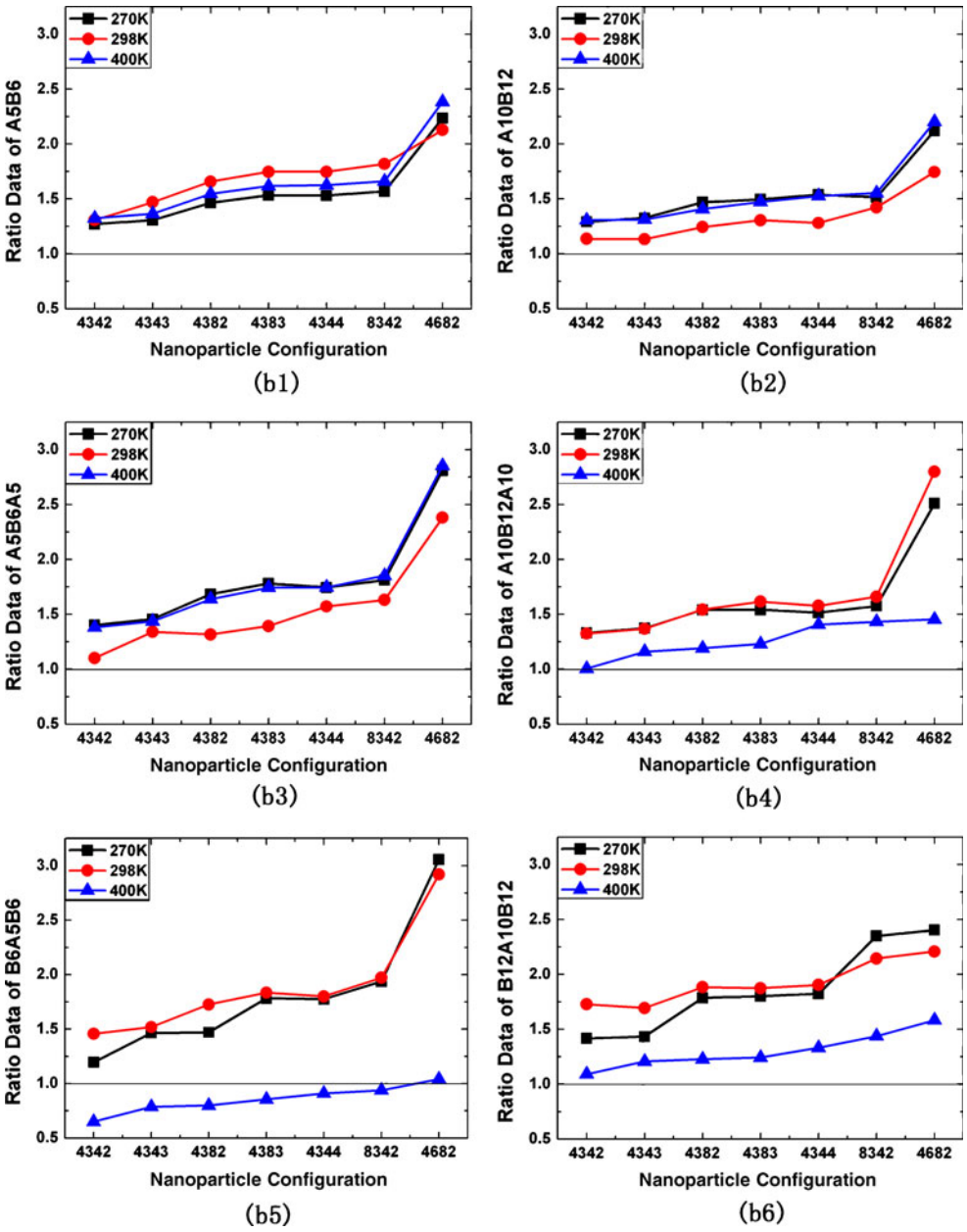

Fig. 5 *R* values of six different PEO-b-PMMA copolymers doped with nanoparticles in various configurations at 270, 298, and 400 K. These data were derived from those shown in Fig. 4

subfigures b2, b3, b4, b5 and b6. The cases where the *R* values showed a different order than that seen at 400 K were termed "defect cases". For example, in subfigure b2, the *R* value for the 4344 system is lower than both 4383 and 8342 values at 298 K, and that for the 8342 system is lower than those for 4344 and 4682 values at 270 K; in subfigure b3, the value for 4344 was lower than those for 4383 and 8342 at 270 K, and the value for 4382 was lower than those for 4343 and 4383 at 298 K; in subfigure b4, the value for 4344 is lower than those for 4383 and 8342 at 270 and 298 K; in subfigure b5, the value of 4344 was lower than those for 4383 and 8342 at 298 K; in subfigure b6, the value of 4343 was lower than those for 4342 and 4382 at 298 K. The number of "defect cases" (those that do not exhibit the same order of *R* values as it was at 400 K) was all small in six subfigures.

There was also a unique feature of Fig. 5. The *R* values were all above the reference line, except the value for the B6A5B6 copolymer. In subfigure b5, the following *R* values were above the reference line: all *R* values at 270 and 298 K, and the *R* values of PEO-b-PMMA copolymers doped with 4682 nanoparticles at 400 K. On the other hand, the other six *R* values were below the reference line. Since most of the *R* values were above the reference line, we could deduce that the nanoparticles had a reinforcing effect on variations in the phase morphology of the PEO-b-PMMA copolymer in most cases (except for the B6A5B6 copolymer at 400 K).

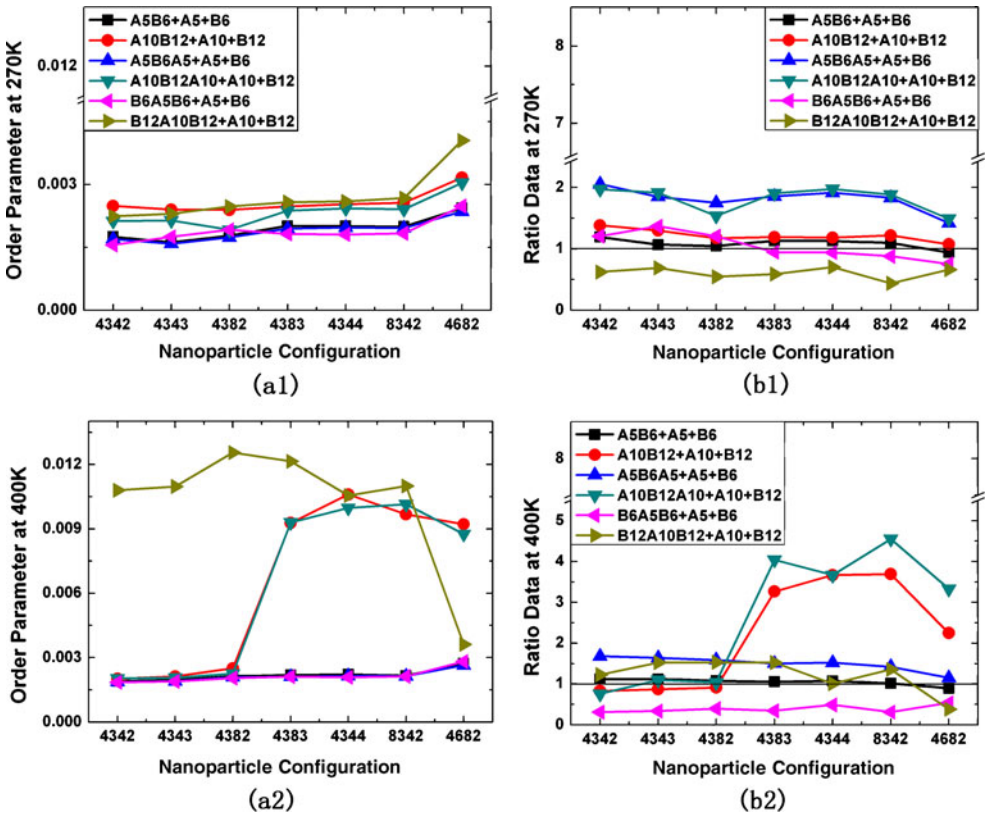

Fig. 6 *P* and *R* values of six different PEO-b-PMMA copolymers doped with both PEO and PMMA as well as nanoparticles (in seven different configurations) at 400 K. The *R* values were derived from the data for the plain PEO-b-PMMA copolymer doped with nanoparticles

Modeling results for PEO-b-PMMA copolymers doped with nanoparticles, PEO, and PMMA

Figure 6 shows the *P* and *R* values of the six PEO-b-PMMA copolymers doped with nanoparticles (in various configurations), PEO, and PMMA at 270 and 400 K. In this case, the *R* values were defined as the *P* value of the PEO-b-PMMA copolymer doped with nanoparticles, PEO and PMMA divided by the *P* value of the PEO-b-PMMA copolymer doped with nanoparticles only. The *P* and *R* values in the four subfigures are arranged in the same order as in Fig. 4 to facilitate comparison between these two figures. We highlight some of the important features of the plots in Fig. 6 below:

(1) In subfigures a1 and b1, the trends in the *P* and *R* values across the different nanoparticle configurations at 270 K were similar for all six PEO-b-PMMA copolymers doped with nanoparticles, PEO, and PMMA. In addition, the trend line for each copolymer was relatively flat, meaning that the nanoparticles had no obvious effect on the PEO-b-PMMA copolymers doped with PEO and PMMA at this relatively low temperature. Furthermore, subfigure b1 indicates the effect of doping with PEO and PMMA: this doping had a weakening effect on B12A10B12 whatever the nanoparticle configuration; it also had a weakening effect on B6A5B6 for the last four nanoparticle configurations, and on A5B6 for the final nanoparticle configuration. The PEO and PMMA doping produced a reinforcing effect in the other cases.

(2) In subfigures a2 and b2, which show the results at 400 K, there were three trend lines (A5B6, A5B6A5 and B6A5B6) that showed similar (flat) trends, even in subfigure a2. Furthermore, subfigure b2 shows the effect of doping with PEO and PMMA, and a weakening effect is noted for the whole B6A5B6 trend line and the final nanoparticle configuration for A5B6. The other copolymers showed reinforcing effects of PEO and PMMA doping at this temperature.

(3) The trend lines of A10B12, A10B12A10 and B12A10B12 in subfigure a2 are rather different: the first six nanoparticle configurations for B12A10B12 and the last four for both A10B12 and A10B12A10 have very high *P* values, which may be due to the high temperature. The extremely high *R* values of the last four nanoparticle configurations for both A10B12A10 and A10B12 may be a combined effect of the copolymer structure, the doping with the homopolymers, and the high temperature. However, A10B12 and A10B12A10 with other nanoparticle configurations showed no effect or even a weakening effect of the homopolymer doping, which (given the

other results) is due to the effect of these particular nanoparticle configurations.

Therefore, if we consider the PEO-b-PMMA copolymers consisting of A10 and B12 components at 400 K, with A10 and B12 homopolymers added as dopants, some of the nanoparticle configurations (4383, 4344, 8342, and 4682) lead to extremely high values of *P*—suggesting that microscopic separation may have occurred—while other nanoparticle configurations (4342, 4343, and 4382) give much lower *P* values (thus suggesting no microscopic separation). The A10 and B12 blocks of the copolymer and the A10 and B12 homopolymers were all longer than A5 and B6, so there would be much more room to form an aggregation area of the same component, and even achieve microscopic separation.

Conclusions

We classified six PEO-b-PMMA copolymers into three groups according to their copolymer structures: "AB", "BAB", and "ABA". In each group, the *P* value of the copolymer with long chains (A10B12, B12A10B12, or A10B12A10) was always higher than that of the copolymer with short chains (A5B6, B6A5B6, or A5B6A5, respectively). The order of *P* values among the copolymers was the same at 270 and 298 K, but it changed markedly at 400 K, especially for the "BAB" group. When doped with either PEO or PMMA homopolymer, these plain copolymers presented different *P* values at certain weight percentages of copolymer. Changing the temperature also produced different effects. At low temperature, the triblock copolymer that had the same component at both ends and was doped with the homopolymer of the copolymer's end component showed the highest *P* and *R* values (i.e., 55% wt. % A5B6A5 doped with A5 and 33% wt.% B6A5B6 doped with B6). At high temperature, the triblock copolymer that had the same component at both ends and was doped with the homopolymer of the copolymer's middle component showed the highest *R* values (i.e., A5B6A5 doped with B6).

We also investigated the plain PEO-b-PMMA copolymers doped with nanoparticles of various sizes, densities, and arrangements via mesoscopic simulations. The simulation results showed that doping with nanoparticles was a good way of improving the degree of order of the mesoscopic phases. The order of *P* values among the nanoparticle configurations was 4682>8342>4344>4383>4382>4343>4342 at 270, 298 and 400 K, and the order of *R* values was nearly the same. Furthermore, the *R* values were all above the reference line, except for B6A5B6 with the first six nanoparticle configurations at 400 K, which means that a more orderly phase morphology can be obtained by increasing the density, size and number of nanoparticles used as dopant. Among these, increasing the size of the nanoparticles was the most efficient method of enhancing the order.

The *P* values of the PEO-b-PMMA copolymer consisting of A10 and B12 blocks at 400 K with A10 and B12 homopolymer dopants were extremely high, indicating that microscopic separation could occur. However, at a relatively low temperature, such as 270 K, doping with these homopolymers did not have a significant effect on the phase morphology.

Acknowledgments This work is supported by the Science–Technology Foundation for Middle-Aged and Young Scientists of Shandong Province (BS2010CL048), a Shandong Province Higher School Science & Technology Fund Planning Project (J10LA61), and a Zaozhuang Scientific and Technological Project (200924-2).

Appendix

This appendix discusses the dynamics and themodynamics of MesoDyn [25].

Dynamics of MesoDyn

The derivation of the diffusive dynamics of the molecular ensemble is based on the assumption that for each type of bead, *I*, the local flux is proportional to the local bead concentration and the local thermodynamic driving force:

$$J_I = -M\rho_I \nabla \mu_I + \widetilde{J}_I,$$

where $\widetilde{J}_I$ is a stochastic flux (which can be thought of as a thermal noise). Combining this with the familiar continuity equation:

$$\frac{\partial \rho_I}{\partial t} + \nabla \cdot J_I = 0$$

leads to simple diagonal functional Langevin equations (that is, stochastic diffusion equations) in the component density fields:

$$\frac{\partial \rho I}{\partial t} = M \nabla \cdot \rho_I \nabla \mu_I + \eta_I$$

A Gaussian distribution of the noise is used. However, the fluctuations in the total density of this simple system are not realistic, since finite compressibility is not enforced by the mean-field potential chosen. Therefore, total density fluctuations are removed by introducing an incompressibility constraint:

$$(\rho_A(r,t) + \rho_B(r,t)) = \frac{1}{v_B},$$

where ν_B is the average bead volume. This condition then leads to the "exchange" Langevin equations:

$$\frac{\partial \rho_A}{\partial t} = Mv_B \nabla\ \rho_A \rho_B \nabla [\mu_A - \mu_B] + \eta$$

and

$$\frac{\partial \rho_B}{\partial t} = Mv_B \nabla \cdot\ \rho_A \rho_B \nabla [\mu_A - \mu_B] + \eta$$

Here, M is a bead mobility parameter, analogous to a self-diffusion coefficient.

The kinetic coefficient $Mv_B\rho_A\rho_B$ models a local exchange mechanism, so the model is only strictly valid for Rouse dynamics. Effects such as repetition lead to kinetic coefficients that extend over a range of roughly the size of the coil. They lead to computationally expensive nonlocal operators which are also very complex in the nonlinear regime.

The distribution of the Gaussian noise satisfies the fluctuation–dissipation theorem $\langle r(r,t)\rangle = 0$ and

$$\langle \eta(r,t)\eta(r'-t')\rangle = -\frac{2Mv_B}{\beta}\delta(t-t')\nabla r \cdot \delta(r-r')\rho_A\rho_B\nabla r'$$

which ensures that time integration of the Langevin equations generates an ensemble of density fields with Boltzmann distributions.

Thermodynamics of MesoDyn

The dynamic Langevin equations contain the bead chemical potential as the thermodynamic driving force of the diffusive dynamics. These chemical potentials can be derived from the thermodynamics of the molecular ensemble. The first step is to derive an expression for the free energy of the system in terms of the bead distribution functions, denoted ψ. The positions of the beads are correlated with each other, making this a multidimensional many-body problem. To overcome this, interchain correlations are neglected, and the system is approximated by a set of independent Gaussian chains embedded in a mean field.

The distribution functions of the independent Gaussian chains factorize exactly, and the density functional can be simplified to a product of single-chain density functionals. In this approximation, the free-energy functional can be written as

$$F[\psi] = \frac{1}{Q}\int dR\left[\psi H^{id} + \beta^{-1}\psi \ln \psi\right] + F^{nid}[\psi]$$

The first term is the average value of the Hamiltonian for the ideal system, comprising the internal Gaussian chain interactions:

$$H^{id} = \sum_{r=1}^{n} H_r^G$$

where H_r^G is the Gaussian chain Hamiltonian of the chain

$$\beta H_r^g = \frac{3}{2a^2}\sum_{s=1}^{n}\left(R_{r,s} - R_{r,s-1}\right)^2$$

Here, α is the Gaussian bond length parameter, and the index s extends over all N segments of the chain. The second term in the free-energy functional stems from the Gibbs entropy of the distributions. The third term is the nonideal contribution related to the interchain interactions. In the present mean-field approximation, the latter is independent of the particular distribution ψ. In the spirit of the particular application of density functional theory taken here (that is, treating the chains as the ideal system), the correlations between the chains are neglected, and the density functional method applies to the correlations within the Gaussian chain only.

The key rudiment of dynamic density functional theory is now that, on a coarse-grained timescale, the distribution function ψ is such that the free-energy functional $F[\psi]$ is minimized. So, ψ is independent of the history of the system, and is fully characterized by the constraints that it represents the density distribution and minimizes the free-energy functional. This constraint on the density fields is realized via an external potential U_I.

Constraint minimization of the free-energy functional leads to an optimal distribution, which in turn—and due to the one-to-one relation between densities, distributions and external potential—can be written

$$\beta F[\rho] = nln\phi + \beta^{-1} lnn! - \sum_I \int U_I(r)\rho I(r)dr + \beta F^{nid}[\rho]$$

Finally, in order to account for the interchain (nonideal) interactions, a Flory–Huggins-type interaction is introduced:

$$\begin{aligned} F^{nid}[\rho] = \frac{1}{2}\int\int & \varepsilon_{AA}(|r-r'|)\rho_A(r)\rho_A(r') \\ & + \varepsilon_{AB}(|r-r'|)\rho_A(r)\rho_B(r') \\ & + \varepsilon_{BA}(|r-r'|)\rho_B(r)\rho_A(r') \\ & + \varepsilon_{BB}(|r-r'|)\rho_B(r)\rho_B(r')drdr' \end{aligned}$$

where $\varepsilon_{ij}(|r-r'|)$ is the mean-field energetic interaction between beads of type i at r and type j at r'. This interaction is defined by the same Gaussian kernel as in the ideal chain Hamiltonian:

$$\varepsilon_{ij}(|r-r'|) = \varepsilon_{ij}^0\left(\frac{3}{2\pi a^2}\right)^{3/2} e - \frac{3}{2a^2}(|r-r'|)^2$$

References

1. Guarini KW, Black CT, Milkove KR, Sandstrom RL (2001) J Vac Sci Technol B 19(6):2784–2788
2. Asakawa K, Hiraoka T, Hieda H, Sakurai M, Kamata Y, Naito K (2002) Jpn J Appl Phys 41(10):6112–6118
3. Mansky P, Chaikin P, Thomas EL (1995) J Mater Sci 30:1987–1992
4. Mansky P, Harrison CK, Chaikin PM, Register RA, Yao N (1996) Appl Phys Lett 68:2586–2588
5. Park M, Harrison CK, Chaikin PM, Register RA, Adamson DH (1997) Science 276:1401–1404
6. Herrninghaus S, Jacobs K, Mecke K, Bischof J, Fery A, Ibn-Elfraj M, Schlagowski S (1998) Science 282:916–919
7. Averopoulos A, Chan VZ-H, Lee VY, No D, Miller RD, Hadjichristidis N, Thomas NL (1998) Chem Mater 10:2109–2115
8. Thurn-Albrecht T, Schotter J, Kastle A, Emley N, Shibauchi T, Krusin-Elbaum L, Guarini K, Black CT, Tuominen MT, Russell TP (2000) Science 290:2126–2129
9. Thurn-Albrecht T, Steiner R, DeRouchey J, Stafford CM, Huang E, Ball M, Tuominen M, Hawker CJ, Russell TP (2000) Adv Mater 12:787–791
10. Black CT, Guarini KW, Milkove KR, Baker SM, Tuominen MT, Russell TP (2001) Appl Phys Lett 79:409–411
11. Seymour RB, Carraher CE (1988) Polymer chemistry. Marcel Dekker Inc., New York
12. Munk P, Aminabhavi TM (2002) Introduction to macromolecular science. Wiley-VCH, New York
13. Carraher CE (2003) Giant molecules: essential materials for everyday living and problem solving. Wiley, New York
14. Mu D, Huang XR, Lu ZY, Sun CC (2008) Chem Phys 348:122–129
15. Patel S, Thakar RS, Wong J, Mcleod SD, Li S (2006) Biomaterials 24:2890–2897
16. Chiu H, Chern CS, Lee CK, Chang HF (1998) Polymer 39:1609–1616
17. Guo SR, Shen LJ, Feng LX (2001) Polymer 42:1017–1022
18. Eisa T, Selfton MV (1993) Biomaterials 14(10):755–761
19. Sun XY, Zhang HL, Zhang LJ, Wang XY, Zhou QF (2005) Polymer 37(2):102–108
20. Valls OT, Farrell JE (1993) Phys Rev E 47:R36–R39
21. Ramirez-Piscina L, Hernandez-Machado A, Sancho JM (1993) Phys Rev B 48:125–131
22. Kawakatsu T, Kawasaki K, Furusaka M, Okabayashi H, Kanaya T (1993) J Chem Phys 99(10):8200–8217
23. Shinozaki A, Oono Y (1993) Phys Rev E 48:2622–2654
24. Calahorra E, Cortazar M, Guzman GM (1985) J Polym Sci Polym Lett Ed 23(5):257–260
25. Accelrys Software, Inc. (2007) Materials Studio online help: MesoDyn. Accelrys Software, Inc., San Diego